Cobalt(II/III) Redox Electrolyte in ZnO Nanowire-Based Dye-Sensitized Solar Cells

Jiandong Fan,[†,‡] Yan Hao,[†,§] Andreu Cabot,*[,‡,⊥] Erik M. J. Johansson,[§] Gerrit Boschloo,*[,§] and Anders Hagfeldt[§]

[‡]Departament d'Electrònica, Universitat de Barcelona, Barcelona, 08028, Spain

[§]Ångström Laboratory, Department of Chemistry, Uppsala University, Box 523, 75120 Uppsala, Sweden

[⊥]Catalonia Institute for Energy Research (IREC), Sant Adria del Besos, Barcelona, 08930, Spain

Supporting Information

ABSTRACT: In this work, we explore the use of cobalt complex redox shuttles in dye sensitized solar cells (DSCs) based on ZnO nanowires (NWs). Arrays of vertically aligned ZnO NWs produced by a low-cost hydrothermal method are used to fabricate DSCs with $[Co(bpy)_3]^{2+/3+}$ as electrolyte. A direct comparison of the performance of $[Co(bpy)_3]^{2+/3+}$-based ZnO DSC with I^-/I_3^--based ones demonstrates the higher suitability of the cobalt complex, both in terms of a larger open circuit voltage (V_{OC}) and a higher photocurrent. The $[Co(bpy)_3]^{2+/3+}$ electrolyte results in V_{OC} enhancements above 200 mV. This V_{OC} increase is associated to the better match between the cobalt complex redox potential and the oxidation potential of the dye. The incident photon-to-current efficiency (IPCE) enhancement is attributed to a less competitive visible light absorption of the cobalt redox couple. Thus the present study opens new opportunities to improve energy conversion efficiency in ZnO-based DSCs.

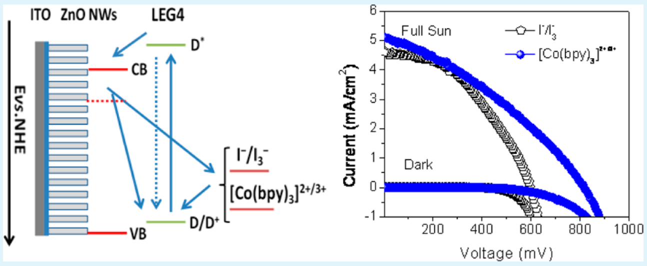

KEYWORDS: *cobalt complex redox shuttles, ZnO nanowires, dye sensitized solar cell, photovoltaics, energy*

INTRODUCTION

Since the first efficient dye-sensitized solar cell (DSC) was demonstrated by O'Regan and Grätzel in 1991,[1] each of its components have been thoroughly analyzed and optimized with the aim to maximize DSCs power conversion efficiency.[2−4] During all this time, the I^-/I_3^- redox shuttle has survived as the best performing electrolyte because it combines a very fast dye regeneration with a slow back reaction of photoinjected electrons with the oxidized redox species. However, the I^-/I_3^- electrolyte has some disadvantages and leaves some room for improvement:[5,6] (i) It is corrosive toward metals such as Ag, Au and Cu, which limits the use of these elements in modules. (ii) It absorbs light in the blue part of the spectrum, lowering the DSC photocurrent and hence the power conversion efficiency. (iii) Its redox potential is not well adjusted to typical sensitizers, which limits V_{OC} in TiO_2-based solar cells to 0.7−0.8 V.[5,7]

Very recently, cobalt(III/II) redox complexes have been demonstrated as excellent alternatives to the I^-/I_3^- redox couple in TiO_2-based DSCs.[8−12] Cobalt(III/II)-based electrolytes offer various advantages over I^-/I_3^-: (i) reduced corrosiveness toward relevant metals; (ii) lower absorption in the visible; and (iii) facile tuning of the redox potential, with the capability to minimize energy loss in the dye regeneration step. In a previous study, we demonstrated that V_{OC} above 900 mV and efficiencies up to 6.7% can be obtained using $[Co(bpy)_3]^{2+/3+}$ in TiO_2-based DSCs.[12] Subsequently, TiO_2-based DSCs employing the $[Co(bpy)_3]^{2+/3+}$ redox couple were reported to reach power conversion efficiency exceeding 12%.[11]

ZnO is the main alternative wide band gap semiconductor to replace TiO_2 as an electron conductor.[13−17] Although a dye optimized to sensitize ZnO-based DSCs remains to be found, ZnO is considered as an excellent backbone to produce high-efficiency DSCs. ZnO has higher bulk electron mobilities than TiO_2. Furthermore, its morphology is easily tunable. This allows the rational design and development of hierarchical ZnO nanostructures able to simultaneously optimize charge carrier path and dye loading.

A particularly advantageous geometry in terms of improving electron transport properties and minimizing recombination during charge carrier transport to the external circuit is that of nanowires (NWs).[18−22] Vertically aligned ZnO NWs can significantly increase the electron diffusion length up to the order of 100 μm.[23,24] Although charge collection efficiencies are already close to 100% in randomly oriented TiO_2 nanoparticles using I^-/I_3^-, NWs may be an advantageous framework structure for DSCs with hole conductors presenting faster recombination, such as Co-based redox couples or solid hole

Received: January 5, 2013
Accepted: February 28, 2013
Published: February 28, 2013

collectors.[11,13,25,26] NWs may also allow getting around one of the drawbacks of bulky cobalt-based redox couples and solid electrolytes: their limited mass transport through structures with narrow pores.[27,28] However, no study has yet reported the use of cobalt-based redox couples on ZnO-based DSCs or NW-based DSCs.

In this work, we explore the performance of the $[Co(bpy)_3]^{2+/3+}$ redox couple on ZnO NWs-based DSCs. We first test the new redox electrolyte using ZnO NW arrays with different lengths. Then, using the exact same NW array and LEG4 dye as sensitizer, we perform a direct comparison of the performance of $[Co(bpy)_3]^{2+/3+}$ and I^-/I_3^- redox couples as electrolytes in ZnO NW DSCs (Scheme 1).

Scheme 1. (a) Schematic Energy Diagram of the ZnO Nanowire Solar Cell Sensitized with LEG4 and Using I^-/I_3^- or $[Co(bpy)_3]^{2+/3+}$ as Electrolyte; (b) Molecular Structure of the LEG4 dye; (c) Molecular Structure of $[Co(bpy)_3]^{2+/3+}$

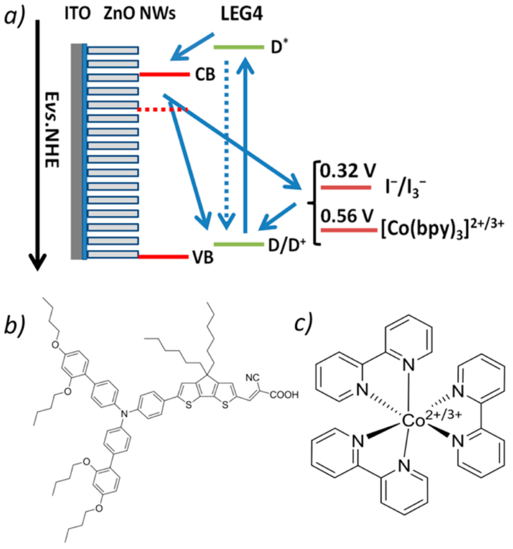

■ EXPERIMENTAL SECTION

Synthesis of ZnO Nanowires. ZnO NWs were obtained by a low-cost, high-throughput, high-yield, and large-area hydrothermal process. First, we sputtered an 80 nm layer of intrinsic ZnO nanoparticle on a glass substrate coated with indium-doped tin oxide (ITO). The intrinsic ZnO layer has a double role: i) it seeds the ZnO NW growth and ii) it blocks the direct contact between the electrolyte and ITO. The ZnO NW growth solution consisted of 0.02 M zinc nitrate, 0.015 M hexamethylenetetramine (HMTA), 0.004 M polyethyleneimine (PEI) (end-capped, molecular weight 800 g/mol LS, Aldrich), and 0.024 M ammonium hydroxide. The seeded substrate was then placed inside 100 mL of the aqueous growth solution. The container was covered and then placed inside a water bath preheated at 88 °C during 3 h. By this procedure, 6 μm long ZnO NWs were obtained. Longer NWs were produced by multiple growth steps, placing the substrate in a fresh zinc nitrate solution every 3 h. The resulting ZnO arrays were rinsed with M.Q water and annealed in Air at 350 °C for 60 min. Surface organic ligands were burned out during this annealing treatment.

DSCs Fabrication. Dye uptake was carried out by immersing the ZnO NWs photoanodes (0.25 cm^2) into an ethanol solution (0.2 mM) of LEG4 (Figure 1) at room temperature for 20 h. A Pt-coated counter electrode was prepared by drop casting a 5 mM H_2PtCl_6 ethanol solution onto an FTO-coated glass, followed by sintering at 450 °C in air for 30 min. A 25 μm thick hot-melt film (Solaronix) was sandwiched between the ZnO NW-based photoanodes and the Pt counter electrode. To complete the device, the electrolyte was injected into the space between the cell's anode and cathode through a hole drilled on the counter electrode. The $[Co(bpy)_3]^{2+/3+}$ electrolyte was obtained by mixing 0.22 M $Co(bpy)_3(PF_6)_2$, 0.05 M $Co(bpy)_3(PF_6)_3$, 0.1 M $LiClO_4$, and 0.2 M 4-tert-butylpyridine (TBP) in acetonitrile. Reference I^- /I_3^- DSCs were prepared using 0.1 M LiI, 0.1 M I_2, 0.2 M TBP, and 0.6 M tetrabutylammonium iodide in acetonitrile.

Characterization. X-ray diffraction (XRD) patterns were obtained with Cu Kα (λ = 1.5406 Å) radiation in a reflection geometry on a Bruker D8 operating at 40 kV and 40 mA. Field-emission scanning electron microscopy (SEM) was used to characterize the morphology of the obtained ZnO NWs. Both cross-section and top-down views were obtained using a FEI Nova NANOSEM 230.

Current−voltage (J-V) characteristics were measured using a Keithley 2400 source/meter and a Newport solar simulator (model 91160) with AM 1.5 G spectral distribution. The intensity power was adjusted to 1000 W m^{-2} using a certified reference solar cell (Fraunhofer ISE). Two neutral density filters were used to reduce intensity to 500 and 100 W m^{-2}. A black mask with an aperture (0.5 × 0.5 cm^2) was placed on top of the cell to avoid any significant contribution from outside of the active area.

Incident photon to current conversion efficiency (IPCE) spectra were recorded using a computer-controlled setup consisting of a xenon light source (Spectral Products ASBXE-175), a monochromator (Spectral Products CM110), and a potentiostat (EG&G PAR 273), calibrated using a certified reference solar cell (Fraunhofer ISE).

Electron lifetime and extracted charge measurements were performed using a white LED (Luxeon Star 1W) as the light source. Voltage and current traces were recorded with a 16-bit resolution digital acquisition board (National Instruments) in combination with a

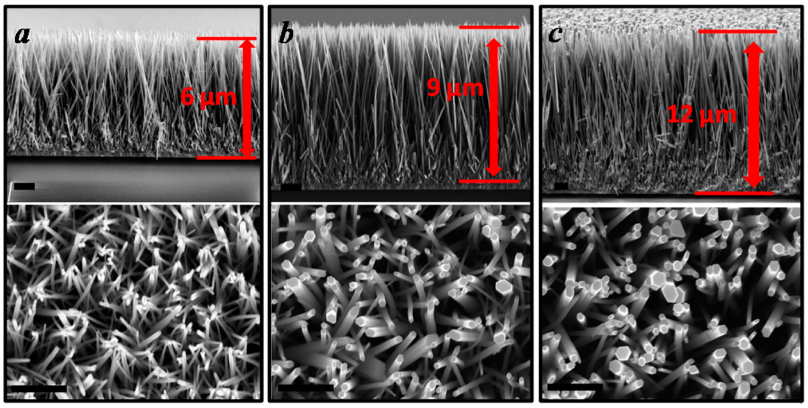

Figure 1. Cross-section and top-down SEM images of ZnO NWs with average length of (a) 6, (b) 9, and (c) 12 μm. All scale bars correspond to 1 μm.

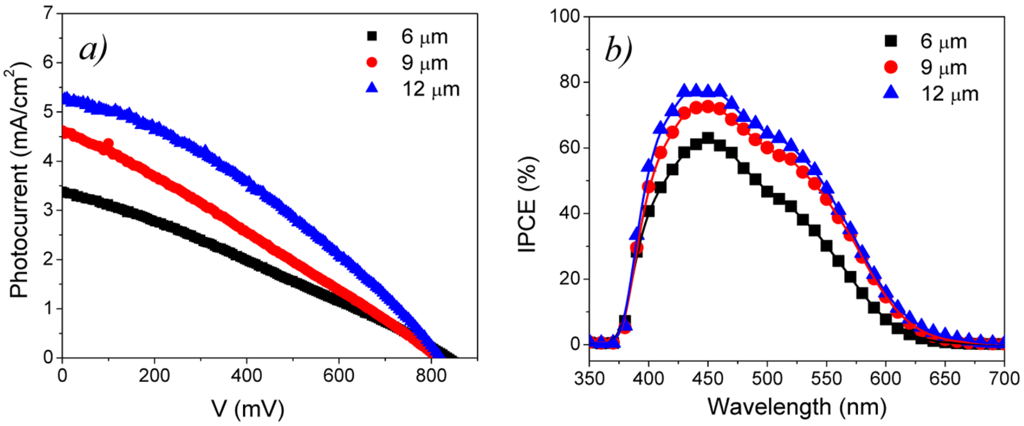

Figure 2. (a) *J*−*V* characteristic and (b) spectra of incident photon to current efficiency under AM1.5G illumination of $[Co(bpy)_3]^{2+/3+}$ DSCs using ZnO NWs with different lengths.

current amplifier (Stanford Research Systems SR570) and a custom-made system using electromagnetic switches. Lifetimes were determined by monitoring photocurrent and photovoltage transients at different light intensities upon applying a small square wave modulation to the base light intensity. Extracted charge measurements were performed by illuminating the cell for 5 s under open-circuit conditions and then turning the lamp off to let the voltage to decay to a voltage V. The cell was then short circuited, and the current was measured under 5 s and integrated to obtain Q (V).

■ RESULTS AND DISCUSSION

Vertically aligned ZnO NWs were prepared by a low-cost, high-throughput, high-yield and potentially large-area hydrothermal process. Figure 1 display top-down and cross-section SEM micrographs of ZnO NWs with average lengths of 6 μm, 9 and 12 μm obtained by this procedure. The diameter of the ZnO NWs increased with the NW length, from 40 to 120 nm. XRD analysis confirmed the obtained ZnO NWs to grow in the (100) direction and to have the wurtzite crystal structure (see the Supporting Information, Figure S2).

For DSCs fabrication, ZnO NWs were sensitized with LEG4 dyes by immersing the ZnO NW arrays (0.25 cm^2) into an ethanol solution (0.2 mM) of LEG4 during 20 h. An FTO-covered glass coated with Pt was used as the counter electrode. Figure 2 displays the *J*−*V* characteristic and the incident photon-to-current efficiency (IPCE) of DSCs fabricated using $[Co(bpy)_3]^{2+/3+}$ as electrolyte and ZnO NWs with different lengths (6 μm −12 μm) as the photoanode. The measured photovoltaic parameters are summarized in Table 1. DSC performance and particularly the collected photocurrent were clearly enhanced when increasing the NW length. This enhancement is explained by the increase in the total surface area and thus of the dye loading in longer NW.[14,15] The maximum power conversion efficiency was obtained for 12 μm ZnO NWs at 1.5%. Notice that when decreasing illumination intensity, higher efficiencies were obtained, up to 2.3% at 100 W/m^2 AM1.5G illumination (Table 1 and Figure S3 in the Supporting Information). The same behavior was observed in previous reports using the cobalt redox couple in DSCs.[11,12]

Table 1. Photovoltaic Parameters of the DSCs Based on ZnO NWs with Different Lengths Using $[Co(bpy)_3]^{2+/3+}$ as electrolyte

length (μm)	light intensity (W/m^2)	V_{oc} (mV)	J_{sc} (mA/cm^2)	FF (%)	PCE (%)
6	1000	835	3.39	28.4	0.80
9	1000	815	4.63	27.2	1.03
12	1000	820	5.23	34.2	1.47
12	500	785	2.75	39.2	1.69
12	100	680	0.70	47.9	2.27

The efficiencies obtained here are higher than values previously reported for equivalent ZnO NW-based DSCs using I^-/I_3^- as electrolyte.[14,15] However, the fill factors (FF) for all ZnO NW DSCs fabricated in the present study were relatively low. The low FFs always obtained in ZnO-based DSCs are generally attributed to a rapid charge carrier recombination at the ZnO-electrolyte interface.[29,30] To solve this problem, it is experimentally proved that the addition of TiO_2 shells to ZnO wire cells results in a considerable improvement in FF.[16,29]

For a direct comparison of the $[Co(bpy)_3]^{2+/3+}$ and I^-/I_3^- electrolyte performances, we fabricated iodine- and cobalt-based DSCs using two pieces of the exact same 10 μm ZnO NW arrays. Figure 3a displays representative *J*−*V* characteristics of I^-/I_3^- and $[Co(bpy)_3]^{2+/3+}$ DSCs. Table 2 summaries the performance parameters of two DSCs obtained from splitting a ZnO NW arrays. Although fill factor (FF) require further improvement, $[Co(bpy)_3]^{2+/3+}$-based DSCs systematically displayed slightly higher photocurrents and much higher V_{OC} than I^-/I_3^--based DSCs. In particular, V_{OC} was significantly improved with the use of $[Co(bpy)_3]^{2+/3+}$, from values around 600 mV obtained with I^-/I_3^- to V_{OC} above 800 mV with $[Co(bpy)_3]^{2+/3+}$. The V_{OC} obtained using $[Co(bpy)_3]^{2+/3+}$ were even higher than those previously measured from ZnO@TiO_2 core−shell NWs.[16,17] The outstanding V_{OC} improvement obtained when using the cobalt-based electrolyte was attributed to the lower potential of the $[Co(bpy)_3]^{2+/3+}$ redox couple when compared with I^-/I_3^- (Scheme 1). The better potential match with the dye ground state allows minimizing the energy loss in the dye regeneration step.

Figure 3b displays the IPCE of ZnO NW-based DSCs with $[Co(bpy)_3]^{2+/3+}$ and I^-/I_3^- redox couples. IPCEs were systematically enhanced with the use of the $[Co(bpy)_3]^{2+/3+}$ instead of I^-/I_3^- electrolyte, especially in the blue region of the visible spectrum (Figure 3b). The enhancement in the wavelength range from 350 nm -450 nm was mainly associated to the reduced light absorption of $[Co(bpy)_3]^{2+/3+}$ in this range.[31]

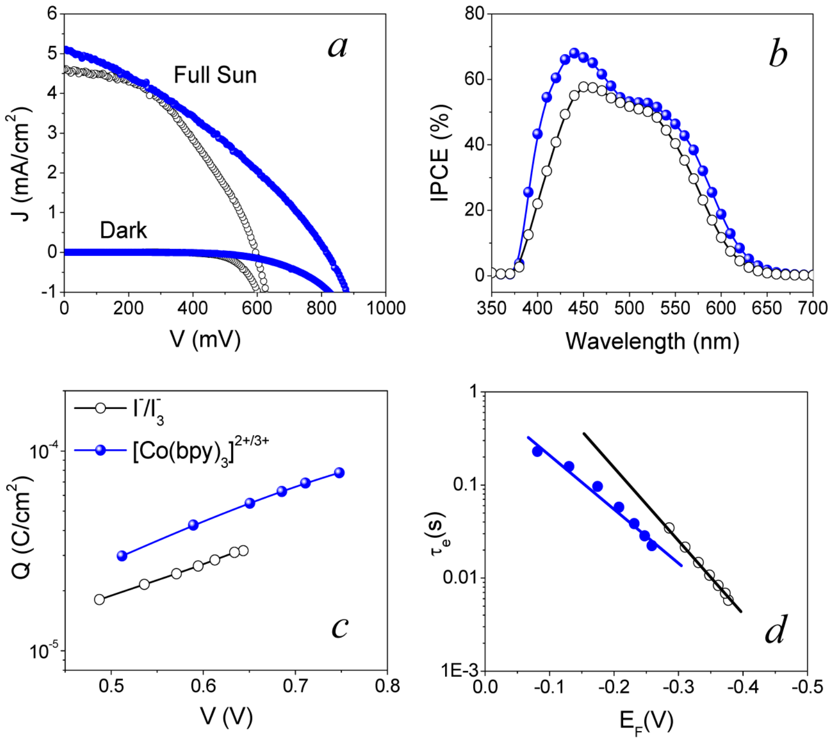

Figure 3. Comparison of ZnO NW DSCs fabricated using I^-/I_3^- (white circle) or $[Co(bpy)_3]^{2+/3+}$ (blue circle) as electrolyte: (a) *J*−*V* characteristic under AM1.5G illumination; (b) spectra of incident photon to current efficiency; (c) charge extraction as a function of voltage under open circuit conditions; (d) electron lifetime as a function of the quasi-Fermi level of the ZnO NW under open circuit conditions for DSCs employing I^-/I_3^- and $[Co(bpy)_3]^{2+/3+}$-based electrolytes, respectively.

Table 2. Photovoltaic Parameters of the DSCs Based on ZnO NWs Using I^-/I_3^- and $[Co(bpy)_3]^{2+/3+}$ as Electrolyte

electrolyte	light intensity (W/m^2)	V_{OC} (mV)	J_{SC} (mA/cm^2)	FF (%)	PCE (%)
I^-/I_3^-	1000	595	4.6	43.5	1.19
$[Co(bpy)_3]^{2+/3+}$	1000	810	5.1	31.1	1.28

We further compared the charge extraction efficiency and charge carrier lifetime in ZnO NW DSCs fabricated using I^-/I_3^- and $[Co(bpy)_3]^{2+/3+}$ electrolytes (Figure 3c, d). Measurements of the extracted charge (Q) were performed by illuminating the cell for 5 s under open-circuit conditions and then turning off the lamp to let the voltage decay to a voltage *V*. The cell was then short circuited, and the current was integrated during 5 s to obtain Q (V). A significant shift of the charge collected from ZnO NW-based DSCs was observed between the I^-/I_3^- and the $[Co(bpy)_3]^{2+/3+}$ electrolyte. The amount of extracted charge at a given voltage was a factor 1.6 higher when using the $[Co(bpy)_3]^{2+/3+}$ electrolyte. This indicated a shift of the electronic states in ZnO toward lower energies with the $[Co(bpy)_3]^{2+/3+}$ electrolyte.

Charge carrier lifetimes were determined by monitoring photovoltage transients at different light intensities upon applying a small square wave modulation to the base light intensity. The measured electron lifetime is plotted as function of the quasi-Fermi level of the ZnO NW under open circuit conditions in Figure 3d. Slightly faster decays were obtained with the use of the $[Co(bpy)_3]^{2+/3+}$ electrolyte. The same behavior was previously observed when the comparison was performed between the I^-/I_3^- and $[Co(bpy\text{-}pz)_2]^{2+/3+}$ electrolytes in TiO_2-based DSCs.7 In our study, it is clear that the electron recombination lifetime is not responsible for the change in voltage. The higher Voc is dominated by the position shift in the redox potential value of the $[Co(bpy)_3]^{2+/3+}$ with respect to the one of the I^-/I_3^- electrolyte.

There is plenty of room for improvement in ZnO NW-based DSCs. We believe the use of $[Co(bpy)_3]^{2+/3+}$ redox electrolyte represents one step in the correct direction, but we speculate that much higher efficiencies can be obtained in $[Co(bpy)_3]^{2+/3+}$-based ZnO NW DSCs by the following modifications: (i) Use longer ZnO NWs and high surface area hierarchical nanostructures to increase dye uptake and enhance photocurrent;[14,16] (ii) coat a TiO_2 shell to improve V_{OC} and fill factor by lowering the rate of electron−hole recombination across the oxide-electrolyte interface;[29,32] (iii) reduce recombination at ZnO surface defects and facilitate dye charge transfer by means of a more severe annealing process and the use of ZnO-based core−shell NW structures;[33,34] (iv) Develop dyes better suited to ZnO surface chemistry;[13] (v) use high surface area−cathode material to reduce charge transfer resistance at the Pt counter electrode and improve fill factor.[7,35−37]

■ CONCLUSIONS

We demonstrated that $[Co(bpy)_3]^{2+/3+}$ offers multiples advantages over I^-/I_3^- to produce efficient ZnO NW-based DSCs. The use of $[Co(bpy)_3]^{2+/3+}$ instead of the conventional I^-/I_3^- electrolyte in ZnO NW-based DSCs resulted in a V_{OC} enhancement of above 200 mV. This was associated to the better match between the $[Co(bpy)_3]^{2+/3+}$ redox potential and the oxidation potential of the dye. ZnO NW-based DSCs obtained with $[Co(bpy)_3]^{2+/3+}$ were also characterized by slightly higher photocurrents. These were associated to a lower light absorption of the $[Co(bpy)_3]^{2+/3+}$ electrolyte in the blue region of visible spectrum. These promising results confirm that cobalt complex redox shuttles are a serious alternative to the conventional I^-/I_3^- redox couple also in ZnO DSCs and represent an important step toward improving energy conversion efficiency in these devices.

ASSOCIATED CONTENT

Ⓢ Supporting Information

SEM images with detailed ITO-ZnO NW interface, XRD pattern of the ZnO NWs, and *J*−*V* characteristics of a ZnO NWs DSC under various light intensities. This material is available free of charge via the Internet at http://pubs.acs.org.

AUTHOR INFORMATION

Corresponding Author

*E-mail: acabot@irec.cat (A.C.); gerrit.boschloo@kemi.uu.se (G.B.).

Author Contributions

[†]J.F. and Y.H. contributed equally to this work

Notes

The authors declare no competing financial interest.

ACKNOWLEDGMENTS

The research was supported by the European Regional Development Funds and the Spanish MICINN Projects MAT2010-15138, MAT2010-21510, CSD2009-00050. J.F. thanks the FI-DGR grant from the Agència de Gestió d'Ajuts Universitaris i de Recerca (AGAUR) from the Catalan Government.

REFERENCES

(1) O'Regan, B.; Grätzel, M. *Nature* **1991**, *353*, 737−740.

(2) Hagfeldt, A.; Boschloo, G.; Sun, L. C.; Kloo, L.; Pettersson, H. *Chem. Rev.* **2010**, *110*, 6595−6663.

(3) Cong, J. Y.; Yang, X. C.; Kloo, L.; Sun, L. C. *Energy Environ. Sci.* **2012**, *5*, 9180−9194.

(4) Tetreault, N.; Grätzel, M. *Energy Environ. Sci.* **2012**, *5*, 8506−8516.

(5) Boschloo, G.; Hagfeldt, A. *Acc. Chem. Res.* **2009**, *42*, 1819−1826.

(6) Gregg, B. A.; Pichot, F.; Ferrere, S.; Fields, C. L. *J. Phys. Chem. B* **2001**, *105*, 1422−1429.

(7) Yum, J.-H.; Baranoff, E.; Kessler, F.; Moehl, T.; Ahmad, S.; Bessho, T.; Marchioro, A.; Ghadiri, E.; Moser, J.-E.; Yi, C.; Nazeeruddin, M. K.; Grätzel, M. *Nat. Commun.* **2012**, *3*, 631.

(8) Wang, M. K.; Grätzel, C.; Zakeeruddin, S. M.; Grätzel, M. *Energy Environ. Sci.* **2012**, *5*, 9394−9405.

(9) Aribia, K. B.; Moehl, T.; Zakeeruddin, S. M.; Grätzel, M. *Chem. Sci.* **2013**, *4*, 454−459.

(10) Mosconi, E.; Yum, J. H.; Kessler, F.; Gomez-Garcia, C. J.; Zuccaccia, C.; Cinti, A.; Nazeeruddin, M. K.; Grätzel, M.; De Angelis, F. *J. Am. Chem. Soc.* **2012**, *134*, 19438−19453.

(11) Yella, A.; Lee, H. W.; Tsao, H. N.; Yi, C. Y.; Chandiran, A. K.; Nazeeruddin, Md. K.; Diau, E. W. G.; Yeh, C. Y.; Zakeeruddin, S. M.; Grätzel, M. *Science* **2011**, *334*, 629−634.

(12) Feldt, S. M.; Gibson, E. A.; Gabrielsson, E.; Sun, L. C.; Boschloo, G.; Hagfeldt, A. *J. Am. Chem. Soc.* **2010**, *132*, 16714−16724.

(13) Anta, J. A.; Guillén, E.; Tena-Zaera, R. *J. Phys. Chem. C* **2012**, *116*, 11413−11425.

(14) Xu, C. K.; Shin, P.; Cao, L. L.; Gao, D. *J. Phys. Chem. C* **2010**, *114*, 125−129.

(15) Qiu, J. J.; Li, X. M.; Zhuge, F. W.; Gan, X. Y.; Gao, X. D.; He, W. Z.; Park, S.-J.; Kim, H.-K.; Hwang, Y.-H. *Nanotechnology* **2010**, *21*, 195602.

(16) Xu, C. K.; Wu, J. M.; Desai, U. V.; Gao, D. *J. Am. Chem. Soc.* **2011**, *133*, 8122−8125.

(17) Wang, M. L.; Wang, Y.; Li, J. B. *Chem. Commun.* **2011**, *47*, 11246−11248.

(18) Law, M.; Greene, L. E.; Johnson, J. C.; Saykally, R.; Yang, P.; Law, M.; Greene, L. E.; Johnson, J. C.; Saykally, R.; Yang, P. *Nat. Mater.* **2005**, *4*, 455−459.

(19) Galoppini, E.; Rochford, J.; Chen, H. H.; Saraf, G.; Lu, Y. C.; Hagfeldt, A.; Boschloo, G. *J. Phys. Chem. B* **2006**, *110*, 16159−16161..

(20) Baxter, J. B.; Aydil, E. S. *Appl. Phys. Lett.* **2005**, *86*, 053114.

(21) Gonzalez-Valls, I.; Lira-Cantu, M. *Energy Environ. Sci.* **2009**, *2*, 19−34..

(22) Baxter, J. B.; Aydil, E. S. *Sol. Energ. Mat. Sol. C.* **2006**, *90*, 607−622..

(23) Martinson, A. B. F.; Goes, M. S.; Fabregat-Santiago, F.; Bisquert, J.; Pellin, M. J.; Hupp, J. T. *J. Phys. Chem. A* **2009**, *113*, 4015−4021.

(24) Martinson, A. B. F.; McGarrah, J. E.; Parpia, M. O. K.; Hupp, J. T. *Phys. Chem. Chem. Phys.* **2006**, *8*, 4655−4659.

(25) Bach, U.; Lupo, D.; Comte, P.; Moser, J. E.; Weissortel, F.; Salbeck, J.; Spreitzer, H.; Gratzel, M. *Nature* **1998**, *395*, 583−585.

(26) González-Vázquez, J. P.; Morales-Florez, V.; Anta, J. A. *J. Phys. Chem. Lett.* **2012**, *3*, 386−393..

(27) Nelson, J. J.; Amick, T. J.; Elliott, C. M. *J. Phys. Chem. C* **2008**, *112*, 18255−18263.

(28) Liberatore, M.; Petrocco, A.; Caprioli, F.; Mesa, C. L.; Decker, F.; Bignozzi, C. A. *Electrochim. Acta* **2010**, *55*, 4025−4029.

(29) Law, M.; Greene, L. E.; Radenovic, A.; Kuykendall, T.; Liphardt, J.; Yang, P. D. *J. Phys. Chem. B* **2006**, *110*, 22652−22663.

(30) Zhang, Q. F.; Chou, T. P.; Russo, B.; Jenekhe, S. A.; Cao, G. Z. *Adv. Funct. Mater.* **2008**, *18*, 1654−1660.

(31) Thomas, W. H. *Dalton Trans.* **2012**, *41*, 3111−3115.

(32) Fan, J. D.; Zamani, R.; Fábrega, C.; Shavel, A.; Flox, C.; Ibáñez, M.; Andreu, T.; López, A. M.; Arbiol, J.; Morante, J. R.; Cabot, A. *J. Phys. D: Appl. Phys.* **2012**, *45*, 415301.

(33) Fan, J. D.; Guell, F.; Fábrega, C.; Shavel, A.; Carrete, A.; Andreu, T.; Morante, J. R.; Cabot, A. *Appl. Phys. Lett.* **2011**, *99*, 262102.

(34) Fan, J. D.; Shavel, A.; Zamani, R.; Fábrega, C.; Rousset, J.; Haller, S.; Güell, F.; Carrete, A.; Andreu, T.; Arbiol, J.; Morante, J. R.; Cabot, A. *Acta Mater.* **2011**, *59*, 6790−6800.

(35) Kavan, L.; Yum, J.-H.; Nazeeruddin, M. K.; Grätzel, M. *ACS Nano* **2011**, *5*, 9171−9178.

(36) Kavan, L.; Yum, J.-H.; Grätzel, M. *Nano Lett.* **2011**, *11*, 5501−5506.

(37) Kavan, L.; Yum, J.-H.; Grätzel, M. *ACS Appl. Mater. Interfaces* **2012**, *4*, 6999−7006.